

A molecular-dynamics study of ductile and brittle fracture in model noncrystalline solids

M.L. Falk*

Department of Physics, University of California, Santa Barbara, CA 93106

(June 26, 2019)

Abstract

Molecular-dynamics simulations of fracture in model amorphous solids are shown to exhibit brittle or ductile behavior depending on small changes in interatomic potential. Yet, simulations of these two model solids under pure shear reveal no significant difference in their flow stress. To understand this change in failure mode we consider the relationship between crack dynamics, rate-dependent plasticity, and molecular-level structures in the glassy solid. In particular these simulations can be understood in the context of Freund and Hutchinson's theory of brittle fracture and the theory of viscoplasticity proposed by Falk and Langer. We also consider a simplified model of the microscopics of plastic deformation as a first-step toward the construction of first-principles models of dynamic plasticity and the brittle ductile transition in noncrystalline materials.

*Present address: Division of Engineering and Applied Sciences, Harvard University, Cambridge, MA 02138; e-mail: falk@esag.harvard.edu

I. INTRODUCTION

This paper presents simulations in which a small change in interatomic potential leads to a qualitative change from ductile to brittle fracture. Our ultimate goal is to understand how brittle or ductile behavior depends on the particulars of the interatomic forces. In order to analyze the results of these simulations in the context of current theories of fracture, we must be able to ask where the material is undergoing plastic deformation. Section III details a technique for calculating a quantitative measure of local non-affine deformation which is applicable to materials with no crystalline order. Using this technique we will pinpoint those areas of the material which are undergoing some molecular level rearrangement akin to a dislocation. After identifying the molecular deformation mechanism, in section IV we consider the connection between current phenomenological theories of brittle and ductile behavior¹ and a theory of this mechanism of molecular level rearrangement in non-crystalline materials developed by Falk and Langer which we shall refer to as FL.² Finally we construct a simplified microscopic model of a deformable region in the solid. This model allows us to relate the intermolecular potential to the parameters which control deformation in FL and translate into the changes of fracture toughness observed in the simulations. Although our current understanding of deformation in amorphous materials is insufficient to develop a first-principles theory for the brittle-ductile transition in noncrystalline materials similar in spirit to theories developed for crystalline materials,^{3–5} this paper attempts to develop some tools and ideas which could pave the way for such a theory in the future.

The concepts of brittleness and ductility are central to any understanding of failure in solids. The most developed first-principles theories of ductility are rooted in the dynamics of dislocations in crystalline solids.^{3–5} Although it has been conjectured that an analog to a crystal dislocation exists in noncrystalline solids,⁶ it remains unclear how to make the direct connection to molecular level phenomena necessary for these theories to be useful in quantitatively understanding transitions between brittle and ductile behavior in disordered materials. In fact, it is not at all clear that a dislocation model of this sort is the most

appropriate way to understand materials without regular structure although these materials are observed to undergo similar brittle-ductile transitions to their crystalline counterparts. We will conjecture here that dislocation concepts are not the most natural way to describe non-crystalline solids, and will attempt to demonstrate that theories of “shear transformation zones” (STZ’s) as first considered in the literature on metallic glasses^{7–12} are a natural way to understand some of the basic physics of brittle versus ductile fracture.

II. SIMULATIONS OF BRITTLE AND DUCTILE FRACTURE IN A NONCRYSTALLINE SOLID

This section describes a series of molecular-dynamics(MD) simulations of fracture in a simple, two-dimensional amorphous solid. While these simulations are examples of brittle and ductile behavior our point here is not simply to differentiate between brittle behavior and ductile behavior, but rather to establish a connection between a particular change in the underlying intermolecular potential and a change in fracture behavior which is measurable as the observed fracture toughness.

From a practical standpoint these studies of brittle and ductile behavior are relevant in the context of several different disordered and amorphous materials. The simulated system is similar in some ways to metallic glasses which have been observed to undergo transitions between ductile and brittle behavior both as a function of temperature and due to small amounts of dilute crystallization produced during annealing.^{13–15} Similar transitions are also critical to the processing of colloidal ceramic systems. These clay-like materials undergo brittle-ductile transitions due to changes in salt content, i.e. changes in interparticle interactions.¹⁶ Issues of brittleness and ductility are also crucial for the production of high-strength polycrystalline metallic alloys in which such transitions have been studied experimentally with respect to temperature and loading rate.¹⁷

A. Methodology

The simulated systems consisted of 90,000 particles in two-dimensions interacting via a two-body potential. In order to avoid problems of local crystallization, a poly-disperse collection of particles was simulated. The system was composed of eight different species in equal proportion with radii from approximately 0.34 to 0.67 units. The radius of each species was 10% larger than the next smallest, and the total volume of the collection was the same as if the particles were all of radius 0.5. This was done to make the system roughly comparable to a single component system in which the rest spacing between two molecules is $r_0 = 1$. The masses of all particles were taken to be $m = 1$.

The inter-molecular potential was different in the two simulations. In the simulation which displayed ductile behavior the potential was a standard Lennard-Jones(LJ) 6-12 potential

$$U_{\alpha\beta}^{LJ}(r) = e \left[\left(\frac{r_\alpha + r_\beta}{r} \right)^{12} - 2 \left(\frac{r_\alpha + r_\beta}{r} \right)^6 \right], \quad (2.1)$$

where r is the interparticle distance and r_α and r_β are the radii of the two particles. e , the depth of the energetic minimum of the two particle interaction, was chosen to be unity. In the simulation which displayed brittle behavior a different potential was used. I will refer to this potential as a Compressed Lennard-Jones(CLJ) potential because it is the standard Lennard-Jones potential rescaled around the center of the potential well,

$$U_{\alpha\beta}^{CLJ}(r) = U_{\alpha\beta}^{LJ}(\lambda r + (1 - \lambda)(r_\alpha + r_\beta)). \quad (2.2)$$

The parameter λ was chosen to be 1.5. This means that width of the potential well was smaller by 33%, and, consequently, the effective range of interaction was also shortened compared to the standard 6-12 Lennard-Jones interaction. For the sake of comparison Fig. 1 shows both potentials. In both cases interactions were cut off at a range of $r_c \approx 2.2r_0$.

All times are given in units of $t_0 = r_0 \sqrt{m/e}$. This unit of time is approximately equivalent to one molecular vibrational period.

The initial amorphous systems were created by taking 10,000-molecule systems and equilibrating them using a sequential MD algorithm with periodic boundary conditions, a Nose-Hoover thermostat^{18–20} and Parrinello-Rahman barostat.^{21,22} The time step in the simulation was taken to be 0.01 time units. The systems were quenched at low temperature while simultaneously being subjected to high pressures in order to create close-packed samples. The samples were then allowed to relax to zero pressure. The ductile sample was observed to have a Young’s modulus of 34 and a shear modulus of 10; the brittle sample was observed to have a Young’s Modulus of 39 and a shear modulus of 12. These 10,000-molecule samples were then used to create larger systems by replicating the small system in a 3×3 array.

The larger systems were simulated via a parallel MD algorithm based on a spatial decomposition method.²³ In order to create the initial conditions for the fracture simulations, the large system was equilibrated for 100 time units while held at a very low temperature, $kT = 0.001e$. A crack was then introduced into the sample. This was accomplished by imposing displacements as determined by the analytical solution for a straight crack in an elastic medium loaded below the ideal critical stress. The faces of the crack were marked so that the top face would not interact with the bottom face to prevent the crack from healing. The outer boundaries of the system were constrained while the simulation was again run to allow the system to relax, holding the temperature constant.

In the fracture simulations no thermostat or barostat was employed. To drive the crack, an initial velocity gradient was imposed across the sample, and the top and bottom surfaces were constrained to move apart vertically such that the side closer to the crack would separate at a strain rate of $0.0001t_0^{-1}$ and the side farthest from the crack would not move apart at all. The horizontal motion of these surfaces was unconstrained. The left and right surfaces were constrained not to move in the horizontal direction, though their vertical motion was unconstrained.

A strain rate of $0.0001t_0^{-1}$ corresponds to a physical strain rate on the order of $10^8 s^{-1}$. While this may seem high compared to typical laboratory values, we can ascertain if there is time for the stresses to equilibrate by multiplying this rate by the time for a sound wave

to traverse the sample, $\approx 300t_0$. The fact that this number is $\approx 0.03 \ll 1$ implies that the system was loaded nearly quasi-statically. That is to say that the loading rate was much slower than the elastic response time, although the loading may not be slow when compared to the time scale for plastic response. Of course, if the crack begins to propagate strain rates near the tip may be significantly higher.

B. Observations

Figure 2 shows the average stress measured during both the brittle and the ductile simulations. In order to better compare the two systems, the stresses are given in units of the critical stress for initial failure of a perfectly brittle solid with the identical elastic properties,

$$\sigma_c = \sqrt{\frac{GE}{\pi a}}. \quad (2.3)$$

Here we assume that, to a good approximation, the system can be treated as a crack in an infinite medium. E is Young's Modulus; a is the initial length of the crack; and G is the energy release rate, which can be expressed as a surface energy and a dissipation per unit crack extension,

$$G = 2\gamma + G_{diss}. \quad (2.4)$$

For an ideally brittle solid all the elastic energy released goes into the creation of new surface, $G_{diss} = 0$. γ was measured by taking a sample of the material in MD, slicing it along an arbitrary plane and measuring the change in potential energy. The value of γ is 1.04 in the CLJ system and 0.94 in the LJ system in units of e/r_0 , thus $\sigma_c^{ideal} = 0.68$ in the ductile system and 0.70 in the brittle system.

Two notable differences are observed between the simulations: (i) In the CLJ simulation, some modest amount of energy was dissipated and the crack began to propagate at about 7% above the ideal brittle critical stress, but in the LJ simulation fracture did not proceed

until the stress was 48% above this value. This means that for the CLJ case the ratio of energy dissipated to the energy expended creating surface is 0.14, while for the LJ case this ratio is 1.19. (ii) In the CLJ simulation, once the crack began to propagate, the stress in the system sharply dipped as the crack moved through the system at speeds reaching 30% of the shear wave speed. Throughout this process the crack tip remained atomically sharp. The process stopped short of releasing all the stress because the crack arrested. In the LJ case, however, the crack tip blunted significantly. In this simulation, the stress remained high while voids nucleated ahead of the tip. The speed of the ductile crack, while difficult to measure due to the mechanism of propagation, stayed well below the speed of the CLJ crack.

III. QUANTIFYING LOCAL DEFORMATION

At this point we have established that the simulation which utilized the CLJ potential Eq. (2.2) resulted brittle behavior while the simulation that utilized the LJ potential Eq. (2.1) resulted in ductile behavior. We expect that the ductility of the LJ simulation resulted from larger amounts of plastic deformation in the vicinity of the crack tip, but we have yet to understand the reason why this particular change in potential resulted in differing amounts of deformation. In order to begin such an analysis we must first establish the nature of the underlying mechanism of deformation. Work by Argon and Spaepen suggests that localized deformations, or “shear transformation zones,” are responsible for rearrangements in these amorphous materials, and in order to satisfy ourselves that this model is the proper one to describe these particular simulations we will examine the microscopic nature of the plastic rearrangement. This will also differentiate the simulations performed here from similar investigations undertaken in crystals^{24,25} where plasticity is observed to be due to dislocations emitted from the crack tip or activated in the vicinity of the crack.

A. Definition of D_{min}^2

In a perfect crystal, dislocations can be readily identified by their characteristic stress fields or as regions of anomalously high potential energy. In glasses, however, such analyses are difficult due to inhomogeneities frozen into the structure. Furthermore, it is not clear that any analog of crystalline dislocations exists in non-crystalline solids. For these reasons, we need some means of identifying regions which deform in a non-affine way in order to observe what sort of microscopic structures play the role of dislocations in these materials.

For the purpose of identifying local rearrangements, we start with a set of molecular positions and subsequent displacements, and compute the closest possible approximation to a local strain tensor in the neighborhood of any particular molecule. To define that neighborhood, we define a sampling radius, which we choose to be the interaction range, r_c . The local strain is then determined by minimizing the mean square difference between the actual displacements of the neighboring molecules relative to the central one, and the relative displacements that they would have if they were in a region of uniform strain ε_{ij} . That is, we define

$$D^2(t, \Delta t) = \sum_n \sum_i \left[r_n^i(t) - r_0^i(t) - \sum_j (\delta_{ij} + \varepsilon_{ij}) (r_n^j(t - \Delta t) - r_0^j(t - \Delta t)) \right]^2, \quad (3.1)$$

where the indices i and j denote spatial coordinates, and the index n runs over the molecules within the interaction range of the reference molecule, $n = 0$ being the reference molecule. $r_n^i(t)$ is the i 'th component of the position of the n 'th molecule at time t . We then find the ε_{ij} which minimizes D^2 by calculating:

$$X_{ij} = \sum_n (r_n^i(t) - r_0^i(t)) \times (r_n^j(t - \Delta t) - r_0^j(t - \Delta t)), \quad (3.2)$$

$$Y_{ij} = \sum_n (r_n^i(t - \Delta t) - r_0^i(t - \Delta t)) \times (r_n^j(t - \Delta t) - r_0^j(t - \Delta t)), \quad (3.3)$$

$$\varepsilon_{ij} = \sum_k X_{ik} Y_{jk}^{-1} - \delta_{ij}. \quad (3.4)$$

The minimum value of $D^2(t, \Delta t)$ is then the local deviation from affine deformation during the time interval $[t - \Delta t, t]$. We shall refer to this quantity as D_{min}^2 .

B. Molecular Level Observations

We have found that D_{min}^2 is an excellent diagnostic for identifying where local rearrangements have taken place. The right-hand frames in Figures 3 and 4 are shaded by the value of D_{min}^2 over the interval from $t = 0$ to the current time. It is immediately apparent that much more non-affine rearrangement takes place in the ductile simulation than in the brittle simulation as we expected. In addition, there seem to develop preferred directions along which deformation takes place. These slip bands which nucleate at the crack tip in the ductile simulation are clear signs that the dynamics of the plastic response and the resulting propagating shear modes are crucial aspects of the problem.

Figure 5 shows one example of a local region before and after rearrangement. This rearrangement took place in the early stages of the ductile simulation prior to significant blunting a small distance in the y-direction from the tip. The arrows denote the sense of the externally applied shear in this region calculated by knowing the asymptotic stress field near a crack tip. The figure illustrates that these regions appear to be of the type discussed by Spaepen as “flow defects”¹⁰ or in other contexts as “shear transformation zones”. That is, the region seems to consist of roughly 10-20 particles, the rearrangements seem to be local, and the “defect” is not mobile in the same sense as a dislocation. Srolovitz, Maeda, Vitek and Egami established that these rearranging regions correspond structurally to “ τ -defects,” regions of anomalously high local shear stress.^{26,27} In the following section we will further explore why these regions are “ τ -defects” and how both the high local stresses and deformation dynamics arise from the particulars of the intermolecular potentials.

IV. ANALYSIS

We would like to understand why this change in interatomic potential leads to a change from brittle to ductile behavior. Unfortunately, our current lack of a detailed understanding of the microscopics of plasticity in non-crystalline materials will prevent us from devising a

detailed first-principles theory of such transitions at this stage. We can, however, draw some important connections between these simulations and current theories of dynamic fracture and the theory of viscoplasticity in amorphous solids presented in FL.² In addition, toward the end of this section we will construct a simplified model of the molecular rearrangements at the heart of the viscoplasticity theory. This model serves to illustrate how we might eventually make connection to first-principles in a theory of this sort.

A. Macroscopic: brittle-ductile behavior

We begin by considering the theory of high strain-rate crack growth developed by Freund and Hutchinson.¹ In this theory the plastic strain rate is considered negligible below some shear stress σ_{flow} and above this stress the strain rate $\dot{\varepsilon}_s^{pl}$ rises linearly.

$$\dot{\varepsilon}_s^{pl} = \dot{\varepsilon}_t + \dot{\varepsilon}_0(\sigma_s - \sigma_{flow})/\mu \quad (4.1)$$

Here μ is the shear modulus, σ_s is the applied shear stress, $\dot{\varepsilon}_t$ is the flow rate at yield and $\dot{\varepsilon}_0$ characterizes the strain rate sensitivity. Furthermore we know that $\dot{\varepsilon}_t \ll \dot{\varepsilon}_0$ and the effect of $\dot{\varepsilon}_t$ will not be important for the purpose of this analysis. Using an assumption of strain rate dominance, the theory finds that the energy release rate of the crack is velocity dependent. Furthermore, the energy release rate of the brittle crack diverges at both high and low velocity. Between these two diverging limits there exists a velocity at which the energy release rate of the crack is a minimum. According to this model the crack cannot propagate when driven at less than this minimum energy release rate. The value of the minimum energy release rate depends on the specifics of the plastic response described in Eq. (4.1) and, by Freund and Hutchinson's analysis

$$\frac{G_{min}}{G_{tip}^c} \approx 1 + \mathcal{C} \frac{\dot{\varepsilon}_0}{\sigma_{flow}^2}, \quad (4.2)$$

where G_{tip}^c is the bare fracture toughness near the tip, and \mathcal{C} is a proportionality constant which depends on the shear modulus, density and G_{tip}^c . [NB: We will ignore a second term proportional to $\dot{\varepsilon}_t/\dot{\varepsilon}_0$ for reasons discussed above.]

In the context of this theory we can ask what would cause one material to propagate a brittle crack while another admits only ductile failure. Since a given mode of failure can only result if a propagating solution exists, we can conjecture that the ductile failure mode results when the propagating brittle solution becomes, for some reason, inaccessible. This implies that the minimum energy release rate for brittle fracture is inaccessible in the ductile material and not in the brittle material. For brittle behavior to have resulted from the narrowing of the inter-particle potential then, the minimum energy release rate should have decreased when the potential well width was narrowed. This further implies that the narrowing of the potential either caused a decrease in $\dot{\varepsilon}_0$, the sensitivity of the strain rate to a change in applied stress, or an increase in σ_{flow} , the critical stress for appreciable plastic flow.

We might at first suspect that we have changed the potential in such a way as to raise the critical stress for plastic flow and this has caused the material to become brittle. This is not the case. Using our molecular-dynamics procedure we can directly measure the stress above which the material begins to flow. Bulk measurements of σ_{flow} obtained by simulating the two systems in periodic boundary conditions with zero applied pressure and a constant applied shear strain rate reveal no significant difference. $\sigma_{flow} \approx 0.4(e/r_0^2)$ for both systems. This implies that a change in the critical flow stress is not the cause of the transition from ductile to brittle behavior in the simulations presented here.

Returning for a moment to the Freund and Hutchinson model, we note that having eliminated σ_{flow} as the responsible parameter for the change in the mode of failure, we must consider the parameter $\dot{\varepsilon}_0$. This parameter corresponds to the sensitivity of the strain rate to an applied stress above the flow stress.

$$\dot{\varepsilon}_0 = \mu \left. \frac{\partial \dot{\varepsilon}_s^{pl}}{\partial \sigma_s} \right|_{\sigma_{flow}^+} \quad (4.3)$$

In order to explore why such a change in $\dot{\varepsilon}_0$ might arise we will now consider a somewhat simplified version of the theory of viscoplasticity in amorphous solids developed in FL.

B. Mesoscopic: viscoplasticity in amorphous solids

In the model of viscoplasticity discussed in FL the plastic flow is both rate and history dependent. The history dependence of the model enters through a set of state variables which describe the density of “shear transformation zones” (STZ) of the type described in section III B. These STZ’s are theorized to be essentially two-state systems and are assumed to have a definite orientation. That is to say that STZ’s that are particularly susceptible to deformation under one sense of shear may not be susceptible to another, and when an STZ undergoes a transition it changes orientation so as to be susceptible to an opposite applied shear stress. For the sake of simplification we assume that locally STZ’s are either aligned perfectly with the applied stress or anti-aligned with the applied stress. Furthermore, we attempt to include the first few non-linear terms which may describe the dynamics of these STZ’s. These terms represent an assumption that inelastic work done on the system may generate new regions or eliminate existing regions.

In FL we related the rate of plastic strain to the rate at which STZ’s transform between their two states,

$$\dot{\varepsilon}_s^{pl} = V_z \Delta\varepsilon [R_+ n_+ - R_- n_-], \quad (4.4)$$

where V_z is the typical volume of a region, $\Delta\varepsilon$ is the increment of local strain due to an individual transformation, n_{\pm} are the population densities of STZ’s in each of the two states, and R_{\pm} are functions of the stress describing the rate at which transitions occur between the two states. The theory also includes equations of motion for the n_{\pm}

$$\dot{n}_{\pm} = R_{\mp} n_{\mp} - R_{\pm} n_{\pm} - C_1 (\sigma_s \dot{\varepsilon}_s^{pl}) n_{\pm} + C_2 (\sigma_s \dot{\varepsilon}_s^{pl}). \quad (4.5)$$

where C_1 and C_2 are constants associated with the non-linear terms which determine the rate of STZ annihilation and creation. We will not revisit the details of these equations except to state that the equations of motion have two steady states: a “jammed” or “hardened” state below the critical stress for plastic flow and a flowing state above this stress. For the flowing steady state

$$n_{\pm} = \frac{C_2}{C_1} \mp \frac{1}{V_z \Delta \varepsilon C_1 \sigma_s}. \quad (4.6)$$

The specifics of our choice of the functions R_{\pm} and their dependence on the stress are important for determining the time dependence of the plastic flow. In FL the transition rates are written as volume activated processes. That is, the rates are written in the form

$$R_{\pm} = R_0 \exp \left[-\frac{\Delta V^*(\pm \sigma_s)}{v_f} \right], \quad (4.7)$$

where for the purpose of this analysis we will assume R_0 to be a constant attempt frequency, v_f is a free volume per particle, and ΔV^* is a free volume needed to activate a transition. The volume needed to activate the transition ΔV^* is a function of the applied shear stress which we chose to have the simplest one parameter functional form for which the volume is assured to be non-negative.

$$\Delta V^*(\sigma_s) = V_0^* \exp(-\sigma_s/\bar{\mu}) \quad (4.8)$$

where V_0^* is the free volume needed to activate a transition at zero stress, and $\bar{\mu}$ is a modulus which characterizes the sensitivity of the activation volume to the applied stress. Having defined these functions we then note that in general $V_0^* \gg v_f$ and these rates are negligible unless $\sigma_s \approx +\bar{\mu}$. Since we are choosing to consider the material response around $\sigma_s = +\sigma_{flow}$, we are in a regime where $R_+ \gg R_-$.

Taking this formulation of the transition rates into account, we can consider the rate of deformation described by Eq. (4.4) in the the steady-state flow regime of Eq. (4.6).

$$\dot{\varepsilon}_s^{pl} \approx V_z \Delta \varepsilon R_+ n_+ = \frac{R_+}{C_1} [\sigma_{flow}^{-1} - \sigma_s^{-1}] \quad (4.9)$$

where $\sigma_{flow} = (C_2 V_z \Delta \varepsilon)^{-1}$. So, we can evaluate $\dot{\varepsilon}_0$ in Eq. (4.3) using Eqs. (4.7-4.9) to be

$$\dot{\varepsilon}_0 = \frac{\mu}{C_1 \sigma_{flow}^2} R_0 \exp \left[-\frac{V_0^*}{v_f} e^{-\sigma_{flow}/\bar{\mu}} \right] \quad (4.10)$$

This last equation provides a first clue as to which aspect of the microscopic behavior is responsible for our observed change from ductile to brittle failure. First we note that we

can reasonably neglect the prefactors to the exponential since the effect of changes in these terms will be substantially less dramatic. Furthermore, the ratio V_0^*/v_f , which we already noted is a large number, is expected to depend primarily on the relative sizes of the particles which are the same in both systems. Since we have already eliminated a substantial change in σ_{flow} , the only remaining parameter in this expression is $\bar{\mu}$. We can see that the double exponential causes $\dot{\varepsilon}_0$ to be suppressed by a factor of $\exp(-V_0^*/v_f)$ when $\bar{\mu}$ becomes large. Moreover Eq. (4.10) is most sensitive to changes in $\bar{\mu}$ when $\bar{\mu} \approx \sigma_{flow}$. The investigations of analogous amorphous systems via computer simulation in FL suggested that $\bar{\mu}$ does indeed fall in this range.

Saying that $\dot{\varepsilon}_0$ is highly sensitive to changes in $\bar{\mu}$ is another way of saying that the sensitivity of the material flow rate to a change in applied shear stress is highly dependent on the sensitivity of the deformable regions (STZ's) in the solid. Relating this to Freund and Hutchinson's fracture model we can state in more prosaic terms that the observed change from ductile to brittle failure seems to be due to a corresponding change from "floppier" to "stiffer" weak regions in the solid. But while the viscoplasticity theory leads us to think in these terms it does not elucidate how we might quantify these ideas and relate them to the molecular potentials.

C. Microscopic: simplified model of a two-state region

We would now like to relate this idea of "floppy" or "stiff" STZ's to a simplified model of molecular rearrangements. The model should be consistent with the observations of Argon, Spaepen and co-workers, i.e. it should be capable of rearranging in a local way,⁷⁻¹¹ and also with the observations made by Srolovitz and co-workers, i.e. it should be a " τ -defect."^{26,27} As a starting point we will ask what the most stripped-down model of our two-state systems might look like on the molecular level. We begin by considering four molecules interacting via a two-body interatomic potential as in Figure 6. Since this unit is embedded in our solid it is constrained from undergoing translation or rotation. For particular choices of the

interatomic potential this four-molecule unit is inherently a two-state system. That is to say that for a Lennard-Jones or similar potential the energy is minimized by having as many bonds near the equilibrium bond length as possible. In this system there are two degenerate ground states, illustrated in Figs. 6(a) and 6(c), in which five of the six bonds are of this length.

Because we associate transitions between the two states of our four-body unit with the development of strain in the solid, we are interested in the rates at which these transitions occur. At high temperatures the transition rates are dominated by rare thermal events which occur only as $\exp(-\Delta U/kT)$, where ΔU is the energy difference between the ground state and the saddle point illustrated in Figure 6(b). This is exactly the approach used to describe the time dependent strain in theories of deformation kinetics such as those of Eyring, Spaepen and Argon.^{28,29,7,11} We cannot use such a formalism here. In our system ΔU is on order unity while kT is three orders of magnitude smaller. Physically this means that we expect our transitions to be driven rather than thermally activated. This is, of course, cause for alarm. The statistical approach of the theories of deformation kinetics in high temperature systems utilized the statistical nature of the energetic fluctuations to discern a time scale. How can we consider a statistical theory when these fluctuations are not relevant? We will instead consider the solid to be composed of an ensemble of these two-state systems, some small fraction of which are close to a free volume induced transition. By using this ensemble picture we hope to preserve the rare-event aspects of transition state theory in order to extract a relevant time scale.

In the previous paragraph and in explaining Eq.(4.7) I have mentioned the concept of a free volume induced transition. In the model of viscoplasticity presented in FL this concept is discussed in some detail, but we have yet to explore what the molecular details of such a transition might look like. In particular, how could we calculate $\Delta V^*(\sigma_s)$, the shear stress dependent free volume needed to activate the transition? In the following paragraphs I will conjecture that since we are interested in driven transitions we must ask the following question: For our model two-state system, constrained by its surroundings to a certain area,

what is the maximum shear that it can support before being driven into a different state? If we can answer this question we can also, given some applied shear stress, determine what free area (our two-dimensional equivalent of free volume) a region must have to become unstable.

With this picture in mind let us consider in some detail what we believe is going on physically. We can parameterize the energy of the four-particle system by only two parameters, its x and y dimensions, if we constrain it from rotating, translating or deforming in an asymmetric way.

$$\mathcal{U}(x, y) = U(x) + U(y) + 4U\left(\frac{1}{2}\sqrt{x^2 + y^2}\right) \quad (4.11)$$

Here U can be any two-particle potential, but we will concern ourselves with U_{LJ} and U_{CLJ} described in section II A. Furthermore we can consider the case when the area (two-dimensional volume) of the system remains constant by imposing the constraint $A = xy$. We can also define a local equivalent shear stress

$$\Sigma_s(x, y) = \frac{1}{2}\left(\frac{1}{y}\frac{\partial \mathcal{U}}{\partial x} - \frac{1}{x}\frac{\partial \mathcal{U}}{\partial y}\right). \quad (4.12)$$

At this point it is possible to understand why such two-state STZ's would be visible as “ τ -defects,” the regions of anomalously high shear stress described by Srolovitz, *et. al.*^{26,27} Consider the condition for the lowest energy of the configuration,

$$\frac{d\mathcal{U}}{ds} = \frac{A}{\sqrt{x^2 + y^2}}\left(\frac{1}{y}\frac{\partial \mathcal{U}}{\partial x} + \frac{1}{x}\frac{\partial \mathcal{U}}{\partial y}\right) = 0, \quad (4.13)$$

where we have traversed the path of constraint by a unit speed curve parameterized by s such that $ds^2 = dx^2 + dy^2$. We immediately note that the condition for equilibrium is **not** the same as the condition for zero shear stress. In general these two conditions are not simultaneously satisfiable. It is important to note that an exception to this, i.e. a case in which the lowest energy configuration has no shear stress, is the case where the molecules interact only via nearest neighbor interactions. This is particularly interesting in light of the simulations since the limit where $\lambda \gg 1$ in Eq. (2.2) is the limit of solely nearest neighbor

interactions. Therefore, we expect that the CLJ potential ($\lambda = 1.5$), which led to brittle fracture in our simulations, should show lower levels of internal shear stresses and fewer “ τ -defects” than the LJ potential ($\lambda = 1$) which in the simulation produced ductile fracture. Thus, the microscopic model strongly suggests that the range of the intermolecular potential is crucial in determining whether these STZ’s are visible as “ τ -defects.”.

We return now to the question of when our two-state STZ will become unstable to an externally applied shear stress. The condition for instability can be written

$$\frac{d\Sigma_s}{ds} = \frac{1}{\sqrt{x^2 + y^2}} \left(x \frac{\partial \Sigma_s}{\partial x} - y \frac{\partial \Sigma_s}{\partial y} \right) = 0 \quad (4.14)$$

where we have again traversed the path of constraint by a unit speed curve. We can now define the equivalent of a free volume in our system, $A_f = A - A_0$. Here A_0 is the equilibrium area of the four-body system at zero applied shear stress $\approx \sqrt{3} (r_0^2)$. In Figure 7 we plot the value of $A_f(\Sigma_s)/A_f(0)$ at which instability sets in for values of the shear stress Σ_s . Because we are interested in understanding the suppression of ΔV^* , and by analogy A_f , as we approach the flow stress, we examine a range of shear stresses up to our observed flow stresses in the fracture samples. This graph looks suggestively similar to the form we had guessed in Eq.(4.8). In actual fact, in the vicinity of $\Sigma_s = 0$, A_f is a power law and not an exponential decay. In order to relate this suppression of the activation volume to values for $\bar{\mu}$ in our viscoplasticity model, we note that the activation area at $\Sigma_s = 0.4$ is 58% of its value at zero in the LJ case and 74% in the CLJ case. This would correspond to $\bar{\mu}_{LJ} = 0.73$ and $\bar{\mu}_{CLJ} = 1.3$. Thus, longer range intermolecular potentials correspond to a solid with “floppier” two-state regions. This result is significant since longer range potentials also implied larger local stresses, and the existence of “ τ -defects.” As we expected from our previous analysis, the toy model with the CLJ potential has a higher value of $\bar{\mu}$ and, therefore, corresponds to a solid with “stiffer” two-state regions. This is in keeping with our expectations since “stiffer” two-state regions should also correspond to a lower value of $\dot{\varepsilon}_0$ and, therefore, by Freund and Hutchinson’s model to a lower minimum energy release rate for brittle fracture from Eq. (4.2). The CLJ solid is observed to undergo brittle fracture.

The analysis presented here is clearly only a first step toward a rigorous first-principles theory of brittle-ductile transitions in noncrystalline solids. Future investigations will hopefully allow more explicit connections to be made between the molecular level structures which are quantifiable via diagnostics such as D_{min}^2 and the observed fracture behavior. Progress will require further developments in our understanding of the molecular physics of deformation in non-crystalline solids.

ACKNOWLEDGMENTS

I would like to acknowledge J.S. Langer for his guidance and encouragement, Alexander Lobkovsky for sharing his ideas and results regarding decohesion models, and A.S. Argon, B.L. Holian, M. Marder and R.L.B. Selinger for helpful discussions. This work was supported by the DOE Computational Sciences Graduate Fellowship Program and DOE Grant No. DE-FG03-84ER45108. The work was also supported in part by National Science Foundation grant CDA96-01954, Silicon Graphics Inc., and the Cornell Theory Center.

REFERENCES

¹ L.B. Freund and J.W. Hutchinson. *J. Mech. Phys. Solids*, 33:169, 1985.

² M.L. Falk and J.S. Langer. *Phys. Rev. E*, 57:7192, 1998.

³ J.R. Rice and R. Thomson. *Phil. Mag.*, 29:73, 1974.

⁴ J.R. Rice. *J. Mech. Phys. Solids*, 40:239, 1992.

⁵ S.J. Zhou, A.E. Carlsson, and R. Thomson. *Phys. Rev. Lett.*, 72:852, 1994.

⁶ J.J. Gilman. *J. App. Phys.*, 44:675, 1973.

⁷ F. Spaepen. *Acta metall.*, 25:407, 1977.

⁸ A.S. Argon. *Acta metall.*, 27:47, 1979.

⁹ A.S. Argon and H.Y. Kuo. *Mat. Sci. Eng.*, 39:101, 1979.

¹⁰ F. Spaepen and A.I. Taub. *Les Houches Lectures XXXV on Physics of Defects*, page 133. North-Holland, Amsterdam, 1981.

¹¹ A.S. Argon and L.T. Shi. *Acta metall.*, 31:499, 1983.

¹² V.A. Khonik and A.T. Kosilov. *J. Non-Cryst. Solids*, 170:270, 1994.

¹³ W.L. Johnson. *Mat. Sci. Forum*, 225:35, 1996.

¹⁴ C.J. Gilbert, R.O. Ritchie, and W.L. Johnson. *App. Phys. Lett.*, 71:476, 1997.

¹⁵ T.-W. Wu and F. Spaepen. *Phil. Mag. B*, 61:739, 1990.

¹⁶ G.V. Franks and F.F. Lange. *J. Am. Ceramic Soc.*, 79:3161, 1996.

¹⁷ R.D. Noebe, C.L. Cullers, and R.R. Bowman. *J. Mater. Res.*, 7:605, 1992.

¹⁸ S. Nose. *J. Chem. Phys.*, 81:511, 1984.

¹⁹ S. Nose. *Molec. Phys.*, 52:255, 1984.

²⁰ S. Nose. *Molec. Phys.*, 57:187, 1986.

²¹ M. Parrinello and A. Rahman. *J. Appl. Phys.*, 52:7182, 1981.

²² M. Parrinello and A. Rahman. *J. Chem. Phys.*, 76:2662, 1982.

²³ S. Plimpton. *J. Comp. Phys.*, 117:1, 1995.

²⁴ S.J. Zhou, P.S. Lomdahl, R. Thomson, and B.L. Holian. *Phys. Rev. Lett.*, 76:2318, 1996.

²⁵ F.F. Abraham, D. Brodbeck, R.A. Rafey, and W.E. Rudge. *Phys. Rev. Lett.*, 73:272, 1994.

²⁶ D. Srolovitz, K. Maeda, V. Vitek, and T. Egami. *Phil. Mag. A*, 44:847, 1981.

²⁷ D. Srolovitz, V. Vitek, and T. Egami. *Acta metall.*, 31:335, 1983.

²⁸ H. Eyring. *J. Chem. Phys.*, 4:283, 1936.

²⁹ A.S. Krausz and H. Eyring. *Deformation Kinetics*. John Wiley & Sons, New York, 1975.

FIGURES

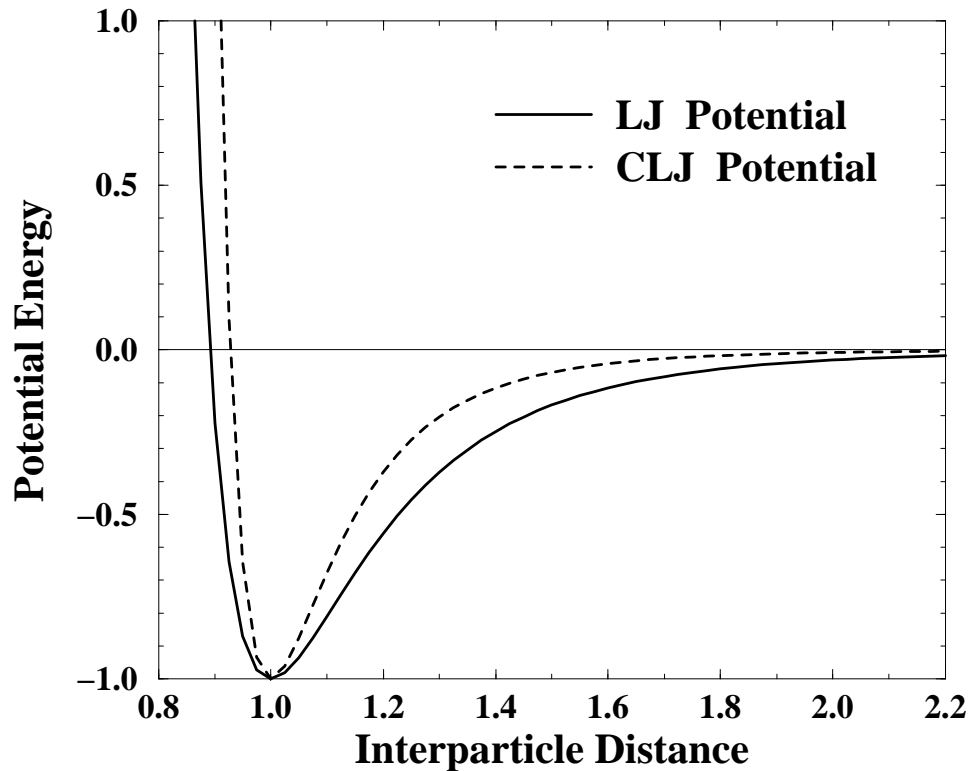


FIG. 1. The LJ and CLJ potentials. Energy is given in units of e . Interparticle distance is given in units of r_0 .

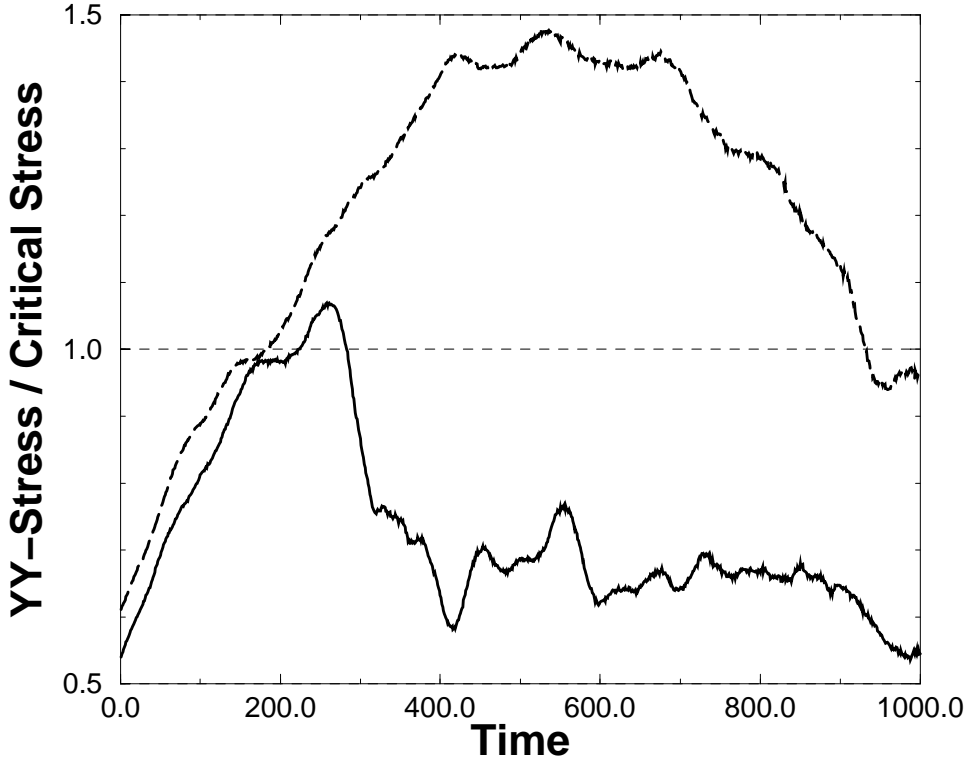


FIG. 2. Stress averaged throughout the sample versus time for the brittle (solid) and ductile (dashed) simulations. The higher stress for the onset of fracture in the ductile case implies increased dissipation. Stresses are given in units of the critical stress for failure of an ideally brittle material with the same elastic properties. Time is given in units of $r_0 \sqrt{m/e}$.

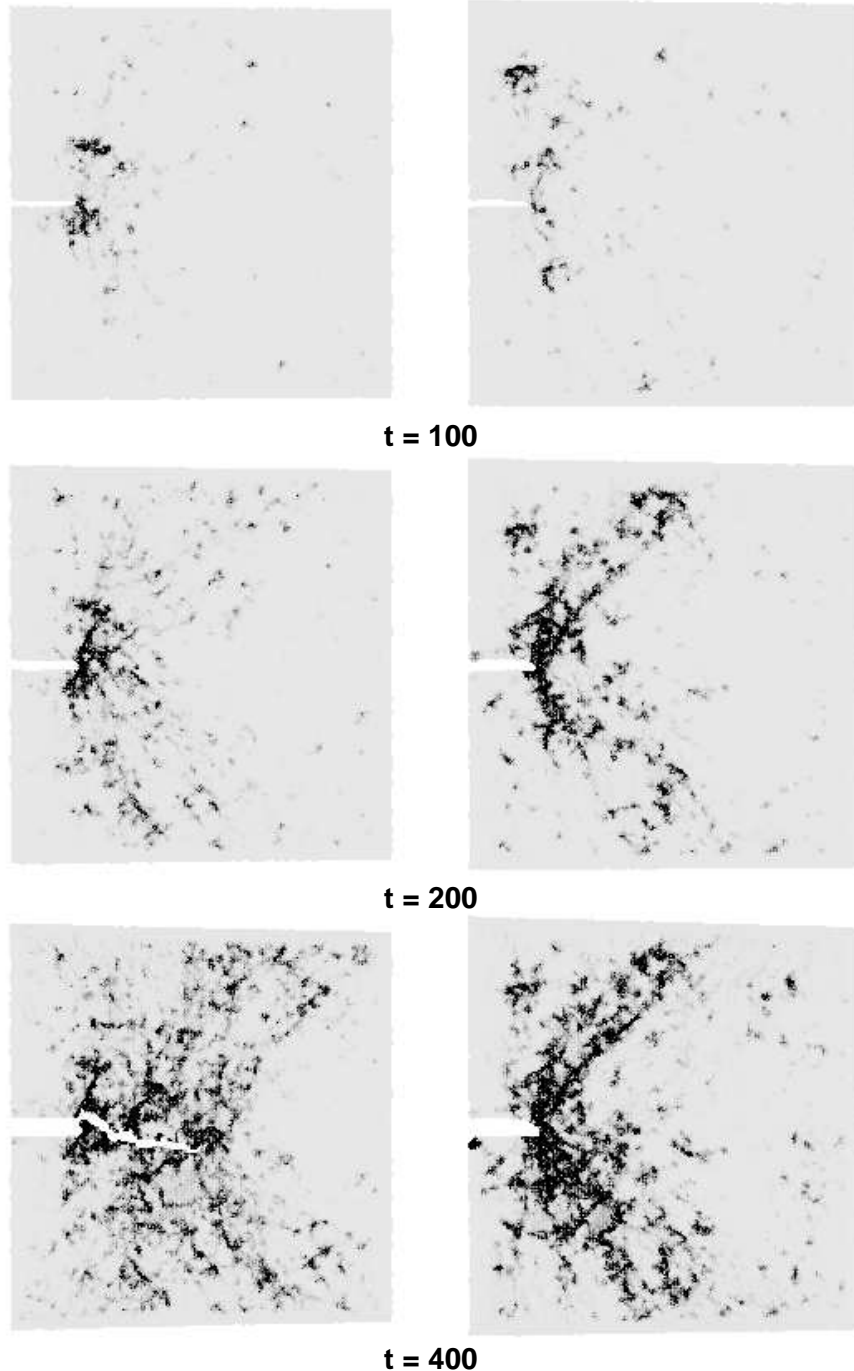


FIG. 3. Frames from the brittle (left) and ductile (right) fracture simulations. In each set the frames are shaded by the parameter D_{min}^2 defined in Eq. (3.1). Dark regions have undergone the highest amount of non-affine rearrangement. The shading saturates when $D_{min}^2 = 1$.

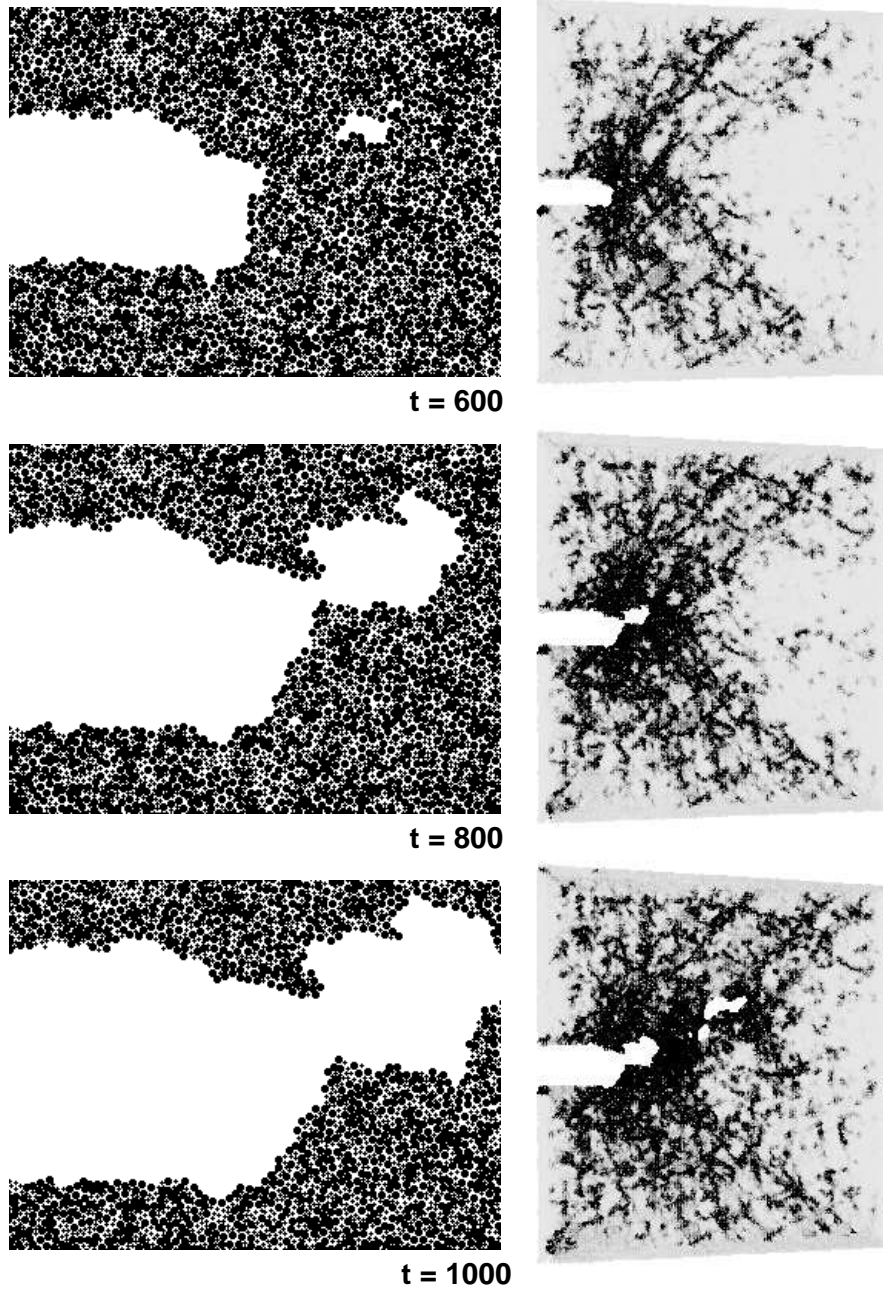


FIG. 4. Frames from the ductile simulation showing the nucleation and growth of a void in the vicinity of the crack tip. The frames on the left are close-ups of the crack tip. The frames on the right are shaded as in Figure 3.

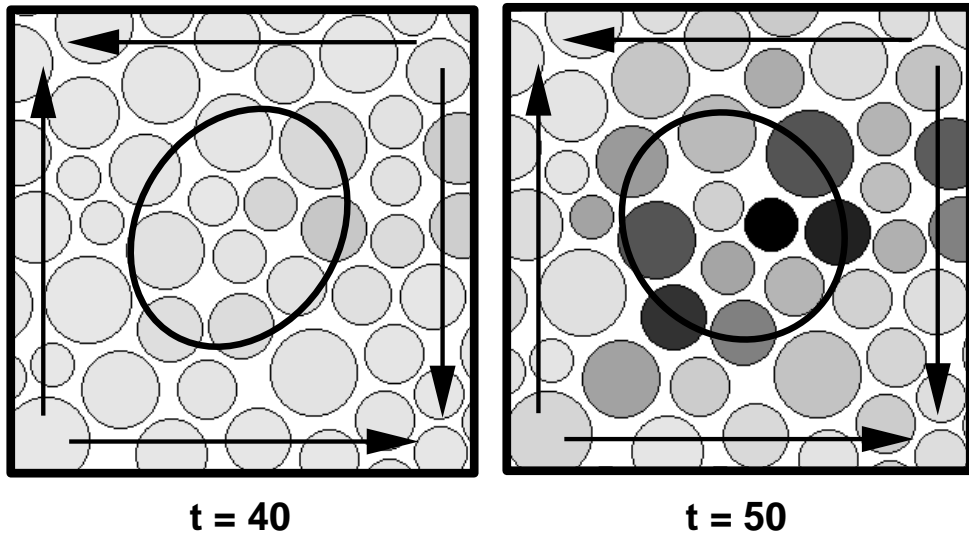


FIG. 5. A local region before and after non-affine rearrangement. The molecules are shaded by D_{min}^2 , the amount of non-affine rearrangement. The arrows denote the approximate direction of the externally applied shear. The ovals are included solely as guides for the eye.

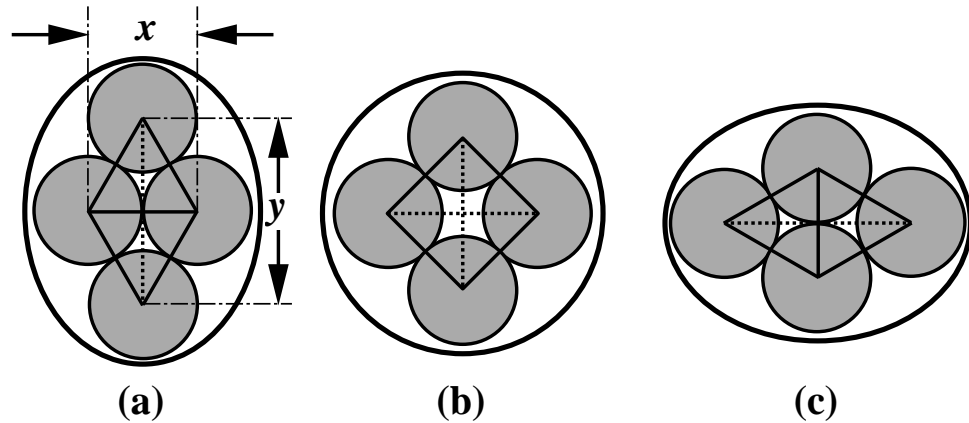


FIG. 6. Diagram of four identical interacting particles making a transition from one stable configuration to another. The middle configuration is the saddle-point configuration for this transition.

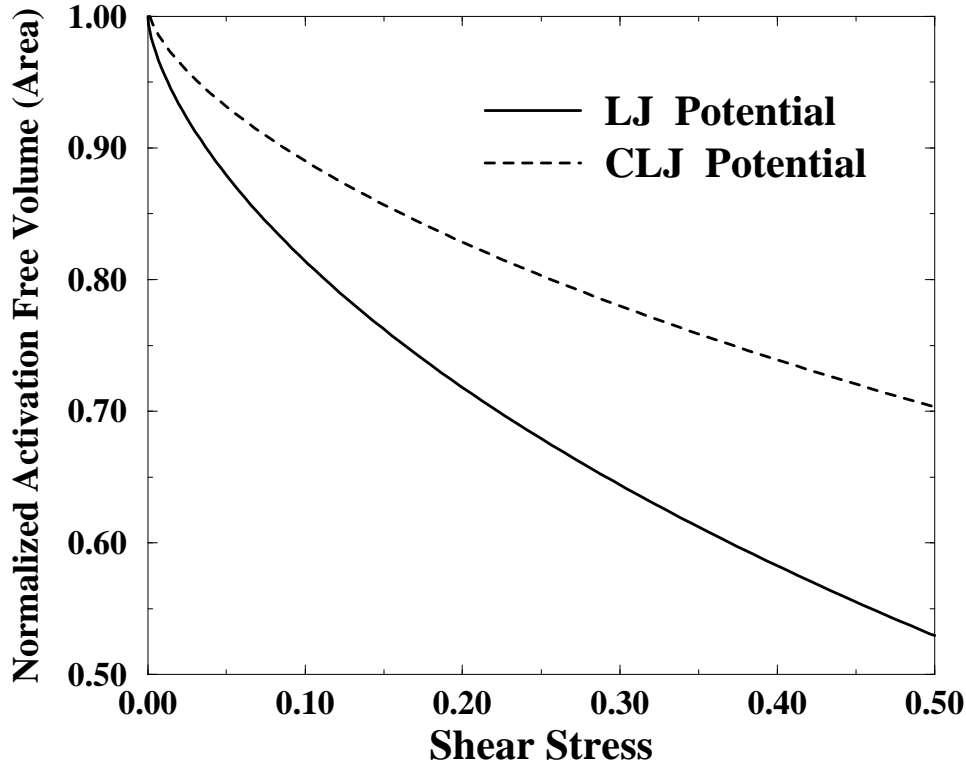


FIG. 7. The activation free volume (area) at shear stress Σ_s divided by the activation free volume (area) at zero applied shear stress, $A_f(\Sigma_s)/A_f(0)$. The activation free volume (area) corresponds to the excess volume at which the four particle system illustrated in Figure 6 becomes unstable to the applied shear. Stresses are given in units of e/r_0^2 .